RESEARCH ARTICLE

On the Mathematical Formalism of the Third-Order Runge-Kutta Method and Its Application to Leukemia Dynamics

Matheus dos Santos Farias[1,*]

[1] Institute for Energy and Nuclear Research (IPEN), University of São Paulo, São Paulo 05508-220, Brazil

Abstract

This paper gives a step-by-step derivation of the classical third-order Runge-Kutta (RK3) method and applies it to a reduced model of leukemia burden under fractionated radiotherapy. Starting from the initial-value problem, the RK3 coefficients are obtained from a third-order Taylor expansion and the resulting order conditions, and the absolute-stability interval of the method on the negative real axis is computed. The biomedical example uses a normalized, subtype-independent burden variable that obeys first-order decay. The treatment schedule (24 Gy in 12 fractions of 2 Gy) is taken from a published case of pediatric extramedullary acute megakaryoblastic leukemia; no patient-specific biological parameters are estimated. The decay rate is prescribed so that one fraction reduces the burden to 0.881 of its initial value, and a normalized three-dimensional Gaussian field is used only for visualization. RK3 and the explicit Euler method are compared with the exact solution of the reduced equation. The observed convergence orders approach 3 for RK3 and 1 for Euler, and the one-fraction step lies well inside the RK3 stability interval. The modeled burden decreases from 0.881 after the first fraction to 0.219 after the twelfth. The application is intended as a methodological illustration, not as a patient-specific prediction.

Keywords: Runge-Kutta method, leukemia dynamics, mathematical modeling, radiotherapy simulation, numerical analysis.

1 Introduction

Leukemia is not a single disease. Acute lymphoblastic leukemia (ALL), acute myeloid leukemia (AML) and chronic myeloid leukemia (CML) are distinct subtypes whose incidence differs markedly by age, sex and world region [1]. A mathematical model of leukemia therefore has to state whether it describes one subtype or only a generic quantity. The published literature covers several subtypes and treatment settings, from early reviews of leukemia and lymphoma models to recent CML models based on ordinary differential equations [2–5]. In the present work the numerical part is generic: the state variable is a normalized

Submitted: 22 July 2026
Revised: 19 August 2026
Accepted: 21 August 2026
Published: 22 November 2026

Vol. 3, **No.** 1, 2027.
10.62762/JNSPM.2026.906286

***Corresponding author:**
✉ Matheus dos Santos Farias
matheusfariasfm@gmail.com

Citation
dos Santos Farias, M. (2026). On the Mathematical Formalism of the Third-Order Runge-Kutta Method and Its Application to Leukemia Dynamics. *Journal of Numerical Simulations in Physics and Mathematics*, 3(1), 73–83.

© 2026 by the Author. Published by Institute of Central Computation and Knowledge. This is an open access article under the CC BY license (https://creativecommons.org/licenses/by/4.0/).

malignant burden, and the derivation of RK3 does not depend on any subtype. The clinical example is taken from a published pediatric case of extramedullary acute megakaryoblastic leukemia, an AML subtype, and is used only to define a realistic treatment schedule. The global burden of the disease is summarized in Figure 1, based on the GLOBOCAN 2022 estimates [6].

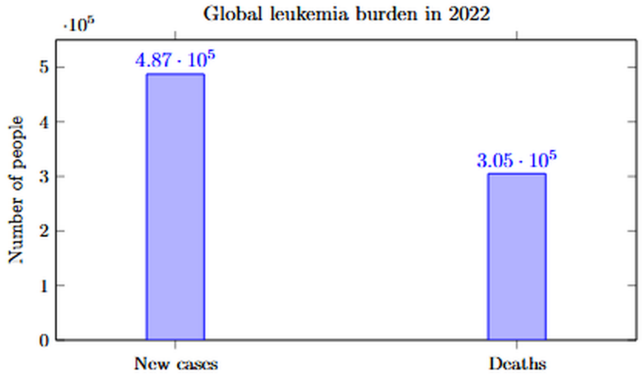


Figure 1. Estimated worldwide numbers of new leukemia cases and leukemia deaths in 2022, based on GLOBOCAN 2022 [6].

To place the study in context, an exploratory search was carried out in PubMed, ScienceDirect, ACL Anthology and Springer Link on 19 August 2026, using combinations of the terms "leukemia", "mathematical modeling", "Runge-Kutta", "RK3", "third-order Runge-Kutta", "numerical simulation", "formal derivation" and "mathematical proof". A record was kept when its title or abstract described a mathematical or numerical leukemia model, a Runge-Kutta-based simulation, or a methodological discussion relevant to the present approach. Duplicates and papers without a clear link to leukemia modeling or numerical simulation were excluded. This was a screening exercise, not a systematic review, so the counts in Figure 2 are descriptive only. One relevant publication was retained from PubMed, two from ScienceDirect, none from ACL Anthology and two from Springer Link. They comprise reviews of mathematical models of leukemia and its treatment, ODE models of chronic myeloid leukemia, and a systematic review of modeling and simulation approaches for designing leukemia treatment technologies [2–5, 7]. None of them gave a full derivation of the classical RK3 scheme before applying it to leukemia, which is the gap addressed here.

The aims of this study are: (i) to derive the classical RK3 formula from the underlying differential problem; (ii) to apply it to a normalized leukemia-burden model;

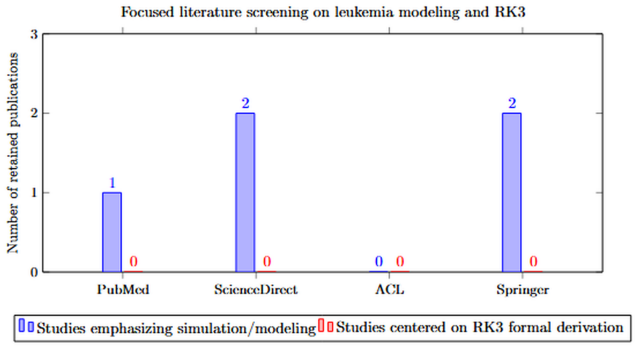


Figure 2. Number of retained publications per database (PubMed, ScienceDirect, ACL Anthology and Springer Link) in the focused screening on leukemia dynamics, Runge-Kutta methods and numerical simulation.

(iii) to verify its convergence against the explicit Euler method; and (iv) to describe the fraction-by-fraction response for a clinically documented radiotherapy schedule.

2 Materials and Methods

The study combines a symbolic derivation, numerical simulation, visualization and a comparison with a published clinical case. The overall workflow is summarized in Table 1. Wolfram Mathematica was used to expand and check the symbolic derivation, MATLAB for the numerical calculations, and Python for the two- and three-dimensional figures. Clinical information was limited to the treatment data reported in the published case of pediatric extramedullary acute megakaryoblastic leukemia [8]. RK3 was used as the main fixed-step method and the explicit Euler method as a first-order baseline. Verification was performed on the reduced burden equation defined below. Because this equation has an exact solution, the global error and the observed order of convergence can be computed directly against it, following standard code-verification practice, instead of relying on visual agreement [9, 10].

3 Mathematical Derivation of the RK3 Method

The RK3 method used here belongs to the family of one-step methods introduced by Carl Runge in 1895 [11]. In 1901 Martin Wilhelm Kutta extended Runge's approach to higher orders and gave, among other schemes, the classical third-order method used in this work [12]. The historical development of these methods is reviewed by Butcher [13].

We begin with the initial-value problem

$$\frac{dy}{dt} = f(t, y), \qquad y(t_0) = y_0, \tag{1}$$

Table 1. Methodological structure of the study.

Stage	Tool / technique	Purpose
Mathematical formalization	Wolfram Mathematica	Expand, simplify and check the Taylor expansions and order conditions of the RK3 derivation.
Numerical simulation	MATLAB	Solve the reduced burden equation, compare the numerical schemes and compute errors and convergence orders.
Clinical data collection	Published case report	Extract the treatment schedule and clinical course reported in the literature to give the simulation a qualitative clinical context.
Scientific visualization	Python	Produce two- and three-dimensional figures of the normalized burden field for each fraction.
Reference numerical method	Explicit Euler method	Provide a first-order baseline for the accuracy comparison.
Main numerical method	Third-order Runge-Kutta method (RK3)	Obtain third-order accuracy at a moderate cost of three function evaluations per step.
Interpretation	Comparative analysis	Relate the numerical trends to the clinically reported course, without claiming clinical validation.
Contribution	Formal derivation and biomedical application	Present the explicit derivation of RK3 and its biomedical application in the same study.

where t is the independent variable, $y(t)$ is the unknown state, $f(t,y)$ is the right-hand side, $h>0$ is the time step, $t_n = t_0 + nh$ are the grid points, and $y_n \approx y(t_n)$ is the numerical approximation at t_n. The RK3 scheme used in the simulations is

$$\begin{aligned} k_1 &= f(t_n, y_n), \\ k_2 &= f\left(t_n + \tfrac{h}{2},\ y_n + \tfrac{h}{2}k_1\right), \\ k_3 &= f(t_n + h,\ y_n - hk_1 + 2hk_2), \end{aligned} \tag{2}$$

and

$$y_{n+1} = y_n + \frac{h}{6}\left(k_1 + 4k_2 + k_3\right). \tag{3}$$

The rest of this section shows how Eq. (3) follows from the differential problem.

Step 1: Exact integral formulation

From Eq. (1),

$$y'(t) = f\big(t, y(t)\big). \tag{4}$$

Integrating over $[t_n, t_n + h]$ and applying the fundamental theorem of calculus,

$$\int_{t_n}^{t_n+h} y'(t)\,dt = \int_{t_n}^{t_n+h} f\big(t, y(t)\big)\,dt, \tag{5}$$

so that

$$y(t_n + h) - y(t_n) = \int_{t_n}^{t_n+h} f\big(t, y(t)\big)\,dt, \tag{6}$$

and therefore

$$y(t_n + h) = y(t_n) + \int_{t_n}^{t_n+h} f\big(t, y(t)\big)\,dt. \tag{7}$$

Equation (7) is exact; a Runge-Kutta method is obtained by approximating the integral with sufficient local accuracy.

Step 2: Taylor expansion of the exact solution up to third order

By Taylor's theorem about t_n,

$$y(t_n+h) = y(t_n) + h\,y'(t_n) + \frac{h^2}{2}y''(t_n) + \frac{h^3}{6}y'''(t_n) + O(h^4). \tag{8}$$

We now compute the derivatives. From Eq. (4),

$$y'(t_n) = f(t_n, y_n), \tag{9}$$

where, for the local truncation analysis, y_n denotes the exact value $y(t_n)$.

For the second derivative we differentiate Eq. (4) with respect to t and apply the chain rule. Here f_t and f_y are the first partial derivatives of $f(t,y)$, and second derivatives are written analogously, e.g. $f_{tt} = \partial^2 f/\partial t^2$, $f_{ty} = \partial^2 f/\partial t\,\partial y$ and $f_{yy} = \partial^2 f/\partial y^2$:

$$y''(t) = \frac{d}{dt} f\big(t, y(t)\big) = f_t(t,y) + f_y(t,y)\frac{dy}{dt}. \tag{10}$$

Using $dy/dt = f(t,y)$,

$$y''(t) = f_t(t,y) + f_y(t,y)\, f(t,y). \tag{11}$$

Differentiating Eq. (11),

$$y'''(t) = \frac{d}{dt}\Big[f_t(t,y) + f_y(t,y)\, f(t,y)\Big], \tag{12}$$

that is,

$$y'''(t) = \frac{d}{dt} f_t(t,y) + \frac{d}{dt}\Big[f_y(t,y)\, f(t,y)\Big]. \tag{13}$$

For the first term, by the chain rule,

$$\frac{d}{dt} f_t(t,y) = f_{tt}(t,y) + f_{ty}(t,y)\frac{dy}{dt}, \tag{14}$$

and, since $dy/dt = f(t,y)$,

$$\frac{d}{dt} f_t(t,y) = f_{tt}(t,y) + f_{ty}(t,y)\, f(t,y). \tag{15}$$

For the second term we use the product rule:

$$\frac{d}{dt}\big[f_y f\big] = \left(\frac{d}{dt} f_y\right) f + f_y \left(\frac{d}{dt} f\right). \tag{16}$$

Again by the chain rule,

$$\frac{d}{dt} f_y(t,y) = f_{yt}(t,y) + f_{yy}(t,y)\, f(t,y), \tag{17}$$

and

$$\frac{d}{dt} f(t,y) = f_t(t,y) + f_y(t,y)\, f(t,y). \tag{18}$$

Substituting Eqs. (17) and (18) into Eq. (16),

$$\begin{aligned}\frac{d}{dt}\big[f_y f\big] &= \big(f_{yt} + f_{yy} f\big) f + f_y\big(f_t + f_y f\big) \\ &= f_{yt} f + f_{yy} f^2 + f_y f_t + f_y^2 f.\end{aligned} \tag{19}$$

Combining Eqs. (15) and (19),

$$y'''(t) = f_{tt} + f_{ty} f + f_{yt} f + f_{yy} f^2 + f_y f_t + f_y^2 f. \tag{20}$$

Assume that $f \in C^3$ in a neighborhood of (t_n, y_n). The mixed partial derivatives are then continuous, and Clairaut's theorem gives $f_{ty} = f_{yt}$; hence

$$y'''(t) = f_{tt} + 2 f_{ty} f + f_{yy} f^2 + f_y f_t + f_y^2 f. \tag{21}$$

Evaluating at $t = t_n$, $y = y_n$ gives

$$y''(t_n) = f_t + f_y f, \tag{22}$$

$$y'''(t_n) = f_{tt} + 2 f_{ty} f + f_{yy} f^2 + f_y f_t + f_y^2 f, \tag{23}$$

where all quantities on the right-hand side are evaluated at (t_n, y_n) and $f = f(t_n, y_n)$.

Substituting Eqs. (9), (22) and (23) into Eq. (8),

$$\begin{aligned}y(t_n + h) = y_n + hf + \frac{h^2}{2}\big(f_t + f_y f\big) \\ + \frac{h^3}{6}\big(f_{tt} + 2 f_{ty} f + f_{yy} f^2 \\ + f_y f_t + f_y^2 f\big) + O(h^4).\end{aligned} \tag{24}$$

Equation (24) is the third-order target that the numerical method must reproduce.

Step 3: General explicit three-stage Runge-Kutta ansatz

We now consider a general explicit three-stage Runge-Kutta method [9]:

$$y_{n+1} = y_n + h\big(b_1 k_1 + b_2 k_2 + b_3 k_3\big), \tag{25}$$

with stages

$$k_1 = f(t_n, y_n), \tag{26}$$

$$k_2 = f\big(t_n + c_2 h,\ y_n + h a_{21} k_1\big), \tag{27}$$

$$k_3 = f\big(t_n + c_3 h,\ y_n + h(a_{31} k_1 + a_{32} k_2)\big). \tag{28}$$

The constants $b_1, b_2, b_3, c_2, c_3, a_{21}, a_{31}, a_{32}$ are chosen so that the expansion of Eq. (25) matches the Taylor series (24).

Step 4: Expansion of the first two stages

From the stage definitions,

$$k_1 = f. \tag{29}$$

Expanding the second stage in a bivariate Taylor series about (t_n, y_n),

$$\begin{aligned}k_2 = f + c_2 h\, f_t + h a_{21} k_1 f_y + \frac{h^2}{2} c_2^2 f_{tt} \\ + h^2 c_2 a_{21} k_1 f_{ty} + \frac{h^2}{2} a_{21}^2 k_1^2 f_{yy} + O(h^3).\end{aligned} \tag{30}$$

Using $k_1 = f$,

$$\begin{aligned}k_2 = f + h\big(c_2 f_t + a_{21} f f_y\big) \\ + h^2\left(\frac{c_2^2}{2} f_{tt} + c_2 a_{21} f f_{ty} + \frac{a_{21}^2}{2} f^2 f_{yy}\right) + O(h^3).\end{aligned} \tag{31}$$

Step 5: Expansion of the third stage

The state argument of k_3 is

$$y_n + h\big(a_{31} k_1 + a_{32} k_2\big). \tag{32}$$

Substituting Eq. (29) and the first-order part of Eq. (31),

$$\begin{aligned} a_{31}k_1 + a_{32}k_2 &= a_{31}f + a_{32}\big[f + h(c_2 f_t + a_{21} f f_y)\big] \\ &\quad + O(h^2) \\ &= (a_{31}+a_{32})f + h a_{32}\big(c_2 f_t + a_{21} f f_y\big) \\ &\quad + O(h^2). \end{aligned} \tag{33}$$

Hence the state argument of f in k_3 is

$$y_n + h(a_{31}+a_{32})f + h^2 a_{32}\big(c_2 f_t + a_{21} f f_y\big) + O(h^3). \tag{34}$$

Expanding k_3 about (t_n, y_n),

$$\begin{aligned} k_3 &= f + c_3 h\, f_t + f_y\Big[h(a_{31}+a_{32})f \\ &\quad + h^2 a_{32}\big(c_2 f_t + a_{21} f f_y\big)\Big] + \frac{1}{2}(c_3 h)^2 f_{tt} \\ &\quad + c_3 h \cdot h(a_{31}+a_{32}) f\, f_{ty} \\ &\quad + \frac{1}{2} h^2 (a_{31}+a_{32})^2 f^2 f_{yy} + O(h^3). \end{aligned} \tag{35}$$

Therefore,

$$\begin{aligned} k_3 &= f + h\big[c_3 f_t + (a_{31}+a_{32}) f f_y\big] \\ &\quad + h^2\Big[a_{32} c_2 f_y f_t + a_{32} a_{21} f_y^2 f + \frac{c_3^2}{2} f_{tt} \\ &\quad + c_3 (a_{31}+a_{32}) f f_{ty} \\ &\quad + \frac{(a_{31}+a_{32})^2}{2} f^2 f_{yy}\Big] + O(h^3). \end{aligned} \tag{36}$$

Step 6: Expansion of the numerical update

Substituting Eqs. (29), (31) and (36) into Eq. (25),

$$\begin{aligned} y_{n+1} &= y_n + h(b_1+b_2+b_3)f \\ &\quad + h^2\big[b_2 c_2 f_t + b_2 a_{21} f f_y + b_3 c_3 f_t \\ &\quad + b_3 (a_{31}+a_{32}) f f_y\big] \\ &\quad + h^3\Big[\frac{b_2 c_2^2}{2} f_{tt} + b_2 c_2 a_{21} f f_{ty} + \frac{b_2 a_{21}^2}{2} f^2 f_{yy} \\ &\quad + b_3 a_{32} c_2 f_y f_t + b_3 a_{32} a_{21} f_y^2 f + \frac{b_3 c_3^2}{2} f_{tt} \\ &\quad + b_3 c_3 (a_{31}+a_{32}) f f_{ty} \\ &\quad + \frac{b_3 (a_{31}+a_{32})^2}{2} f^2 f_{yy}\Big] + O(h^4). \end{aligned} \tag{37}$$

For third-order consistency, Eq. (37) must agree with Eq. (24). Matching the coefficients term by term gives the order conditions

$$b_1 + b_2 + b_3 = 1, \tag{38}$$

$$b_2 c_2 + b_3 c_3 = \tfrac{1}{2}, \tag{39}$$

$$b_2 a_{21} + b_3 (a_{31}+a_{32}) = \tfrac{1}{2}, \tag{40}$$

$$b_2 c_2^2 + b_3 c_3^2 = \tfrac{1}{3}, \tag{41}$$

$$b_2 c_2 a_{21} + b_3 c_3 (a_{31}+a_{32}) = \tfrac{1}{3}, \tag{42}$$

$$b_2 a_{21}^2 + b_3 (a_{31}+a_{32})^2 = \tfrac{1}{3}, \tag{43}$$

$$b_3 a_{32} c_2 = \tfrac{1}{6}, \tag{44}$$

$$b_3 a_{32} a_{21} = \tfrac{1}{6}. \tag{45}$$

Step 7: Selection of the classical RK3 coefficients

The classical explicit RK3 method is obtained by choosing

$$c_2 = \tfrac{1}{2}, \quad c_3 = 1, \quad a_{21} = \tfrac{1}{2}, \quad a_{31} = -1, \quad a_{32} = 2, \tag{46}$$

so that

$$a_{31} + a_{32} = 1. \tag{47}$$

From the third-order condition (44),

$$b_3 \cdot 2 \cdot \tfrac{1}{2} = \tfrac{1}{6} \;\Rightarrow\; b_3 = \tfrac{1}{6}. \tag{48}$$

From the second-order condition (39),

$$b_2 \cdot \tfrac{1}{2} + \tfrac{1}{6} \cdot 1 = \tfrac{1}{2} \;\Rightarrow\; \tfrac{b_2}{2} = \tfrac{1}{3} \;\Rightarrow\; b_2 = \tfrac{2}{3}. \tag{49}$$

Finally, from the first-order condition (38),

$$b_1 + \tfrac{2}{3} + \tfrac{1}{6} = 1 \;\Rightarrow\; b_1 = 1 - \tfrac{5}{6} = \tfrac{1}{6}. \tag{50}$$

The remaining conditions are then satisfied as well: Eq. (40) gives $\frac{2}{3}\cdot\frac{1}{2} + \frac{1}{6}\cdot 1 = \frac{1}{2}$; Eq. (41) gives $\frac{2}{3}\cdot\frac{1}{4} + \frac{1}{6}\cdot 1 = \frac{1}{3}$; Eq. (42) gives $\frac{2}{3}\cdot\frac{1}{4} + \frac{1}{6}\cdot 1 = \frac{1}{3}$; Eq. (43) gives $\frac{2}{3}\cdot\frac{1}{4} + \frac{1}{6}\cdot 1 = \frac{1}{3}$; and Eq. (45) gives $\frac{1}{6}\cdot 2\cdot\frac{1}{2} = \frac{1}{6}$. All eight conditions hold, so the method is of third order. The coefficients are

$$\begin{aligned} &b_1 = \tfrac{1}{6}, \quad b_2 = \tfrac{2}{3}, \quad b_3 = \tfrac{1}{6}, \\ &c_2 = a_{21} = \tfrac{1}{2}, \quad c_3 = 1, \quad a_{31} = -1, \quad a_{32} = 2. \end{aligned} \tag{51}$$

Step 8: Recovery of the final RK3 formula

Substituting Eq. (51) into the general stage definitions,

$$k_1 = f(t_n, y_n), \tag{52}$$

$$k_2 = f\big(t_n + \tfrac{h}{2},\; y_n + \tfrac{h}{2} k_1\big), \tag{53}$$

$$\begin{aligned} k_3 &= f\big(t_n + h,\; y_n + h(-k_1 + 2k_2)\big) \\ &= f\big(t_n + h,\; y_n - h k_1 + 2h k_2\big), \end{aligned} \tag{54}$$

and the update becomes

$$y_{n+1} = y_n + h\left(\tfrac{1}{6}k_1 + \tfrac{2}{3}k_2 + \tfrac{1}{6}k_3\right). \tag{55}$$

With the common denominator 6,

$$y_{n+1} = y_n + \frac{h}{6}\big(k_1 + 4k_2 + k_3\big). \tag{56}$$

These expressions are identical to Eqs. (2) and (3).

Step 9: Interpretation of the variables and stability

In Eqs. (2)–(3), t_n is the current time node, h is the step size, y_n is the known approximation of the state at t_n, and k_1, k_2 and k_3 are successive slope evaluations. The first stage gives the slope at the start of the interval, the second an estimate at the midpoint, and the third a slope at the end of the interval obtained from a combination of the first two. Their weighted average yields a third-order approximation of the exact solution.

The absolute stability of the method follows from its stability function [9]. For the linear test equation $y' = \lambda y$, RK3 gives $y_{n+1} = R(z)\, y_n$ with

$$R(z) = 1 + z + \frac{z^2}{2} + \frac{z^3}{6}, \qquad z = h\lambda, \tag{57}$$

and absolute stability requires $|R(z)| \leq 1$. On the negative real axis this condition gives approximately the interval $-2.5127 \leq z \leq 0$. For a decaying scalar mode with $\lambda = -\kappa$ the step-size condition is therefore $h\kappa \leq 2.5127$. In the reduced burden model used here, $\kappa = 0.12670\ \text{fraction}^{-1}$, which gives $h \leq 19.83$ fractions; the adopted step $h = 1$ fraction lies well inside this interval. For a multi-compartment model the same condition would have to be checked for the eigenvalues of the Jacobian, not inferred from the scalar case. Because the scheme is derived from the Taylor structure of the differential problem, each step of the computation can be traced back to the continuous model.

4 Clinical Reference and Scope of the Application

The clinical reference is the case report by Gutiérrez-Jimeno et al. [8], which describes a 7-month-old girl with extramedullary acute megakaryoblastic leukemia and an atypical presentation with skull bone lesions. She was treated according to the NOPHO-DBH AML 2012 protocol with two induction cycles and one consolidation cycle, followed by external radiotherapy to the skull (24 Gy in 12 fractions of 2 Gy). The main parameters extracted from the report are listed in Table 2. The case provides a documented schedule on which a fraction-indexed numerical experiment can be built. The model does not estimate subtype-specific proliferation, apoptosis or radiosensitivity, nor any patient-specific biological parameter: the clinical case defines only the timing of the treatment, while the mathematical model describes a normalized burden variable. The simulation should therefore not be read as a calibrated mechanistic model of acute megakaryoblastic leukemia; its purpose is to verify the numerical method in a clinically realistic setting.

Table 2. Clinical and therapeutic parameters extracted from the selected case report [8].

Parameter	Value reported in the article
Article	Gutiérrez-Jimeno et al. (2022), *Frontiers in Pediatrics*
Patient profile	Female; 7 months old at diagnosis; 18 months old at death
Disease type	Extramedullary acute megakaryoblastic leukemia (eAML)
Initial manifestation	Skull bone lesions; persistent extramedullary disease
Initial protocol	NOPHO-DBH AML 2012
Induction treatment	2 induction cycles (MEC; ADxE)
Consolidation treatment	1 consolidation cycle (HAM)
Radiotherapy site	Skull
Radiotherapy total dose	24 Gy
Number of fractions	12
Dose per fraction	2 Gy
Radiation schedule	Fractionated external radiotherapy; weekly frequency not reported
Indication for radiotherapy	Persistent extramedullary disease after induction and consolidation
Salvage treatment	2 courses of salvage chemotherapy: CLO (clofarabine) and FLA (fludarabine)
Chemotherapy doses	Not reported
Transplant procedure	Haploidentical CD45RA$^+$ lymphocyte-depleted hematopoietic stem cell transplantation
Clinical course	Persistent extramedullary disease; progression despite intensive treatment
Outcome	Death from disease progression in August 2021

5 Reduced Leukemia-Burden Model and Initialization

The biomedical application uses a normalized burden variable $B(t)$ instead of an absolute cell count. The model is subtype-independent and converts the

Table 3. Convergence of RK3 and explicit Euler for the reduced leukemia-burden model at $t = 12$ fractions.

h (fraction)	RK3 $B(12)$	RK3 error	RK3 order	Euler $B(12)$	Euler error	Euler order
1.000	0.218599400	3.12×10^{-5}	–	0.196777540	2.19×10^{-2}	–
0.500	0.218626873	3.70×10^{-6}	3.07	0.207907022	1.07×10^{-2}	1.03
0.250	0.218630126	4.51×10^{-7}	3.04	0.213318032	5.31×10^{-3}	1.01
0.125	0.218630521	5.57×10^{-8}	3.02	0.215986430	2.64×10^{-3}	1.01

12-fraction schedule into a reproducible numerical experiment. The burden is assumed to follow first-order decay, the simplest model that produces a monotonically decreasing burden:

$$\frac{dB}{dt} = -\kappa B(t), \qquad B(0) = 1. \tag{58}$$

Here $B(t)$ is the normalized malignant burden, t is measured in treatment fractions and κ is an effective decay rate. The value of κ is prescribed so that one fraction reduces the burden to $B(1) = 0.881$, which gives $\kappa = -\ln(0.881) = 0.12670$ fraction^{-1}. The exact solution is

$$B(t) = \exp(-\kappa t), \tag{59}$$

so that $B(12) = \exp(-12\kappa) = 0.21863$, i.e. 0.219 to three decimal places.

For the three-dimensional visualization, the initial spatial distribution $\rho(x, y, z, 0)$ is a normalized Gaussian field centered at the origin, with maximum value 1, standard deviation $\sigma = 10$ spatial units, and computational domain $-30 \le x, y, z \le 30$:

$$\rho(x, y, z, 0) = \exp\left[-\frac{x^2 + y^2 + z^2}{2\sigma^2}\right], \qquad \sigma = 10. \tag{60}$$

The Gaussian field gives a compact central burden that decreases smoothly with radius; it is not meant to reproduce the patient's anatomy. No patient imaging or volumetric burden measurements were used. The clinical case supplies the treatment schedule, whereas the spatial geometry and the normalized field are modeling assumptions made for illustration.

6 Results and Discussion

6.1 Numerical convergence and comparison with Euler's method

The reduced model was solved with RK3 and the explicit Euler method for $h = 1$, 0.5, 0.25 and 0.125 fractions. Since the exact value $B(12) = 0.218630577$ is known, the global error E_h at $t = 12$ can be computed directly, and the observed order is $p = \log_2(E_h/E_{h/2})$. The results in Table 3 show orders of 3.02–3.07 for RK3 and 1.01–1.03 for Euler, as expected from theory. At $h = 1$ the RK3 error (3.12×10^{-5}) is about 700 times smaller than the Euler error (2.19×10^{-2}).

6.2 Fraction-by-fraction response

The numerical experiment follows the 12-fraction schedule reported by Gutiérrez-Jimeno et al. [8]. Because the case report does not include three-dimensional imaging for each fraction, the controlled Gaussian field described above is used. The global burden B does not depend on the color normalization of the point clouds and is therefore the quantity used to compare fractions.

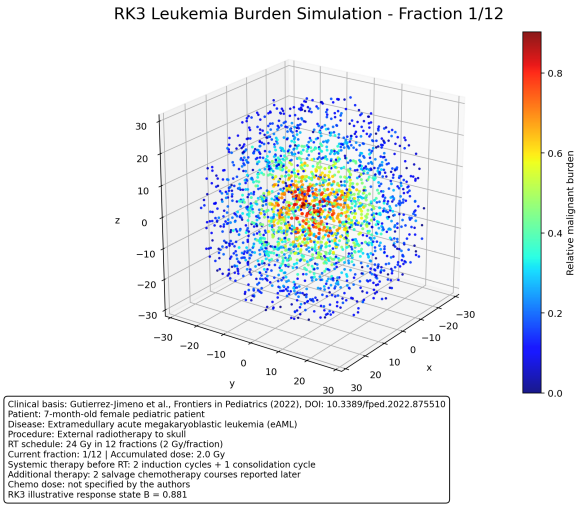


Figure 3. Fraction 1 of 12: simulated burden after 2.0 Gy. Normalized global burden $B = 0.881$.

In each of Figures 3–14, the colorbar gives the local relative burden and the annotation box gives the global normalized burden B for that fraction. The color range is normalized separately in each frame, so color alone cannot be compared across frames; the values of B, together with $B(0) = 1$, provide the quantitative reference. The main numerical result is the decrease of B from 0.881 after the first fraction to 0.219 after the twelfth.

Figures 3 and 4 show the start of treatment. After the first fraction the central red-orange region is broad and dense, corresponding to a high modeled burden.

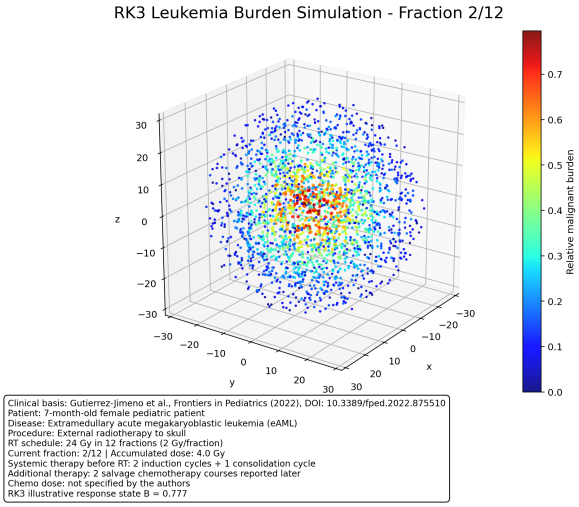


Figure 4. Fraction 2 of 12: early reduction after 4.0 Gy. Normalized global burden $B = 0.776$.

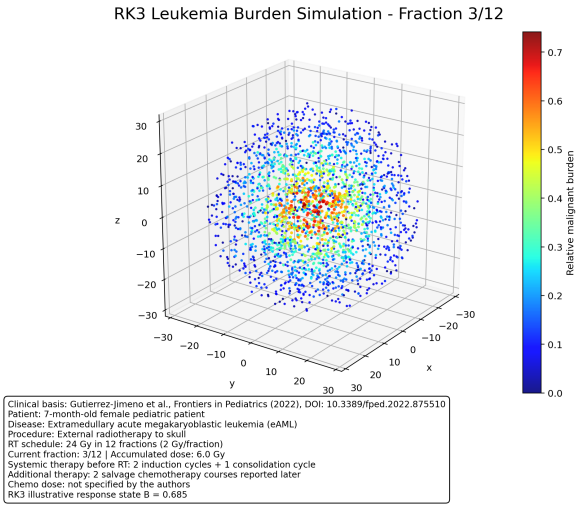


Figure 5. Fraction 3 of 12: progressive reduction after 6.0 Gy. Normalized global burden $B = 0.684$.

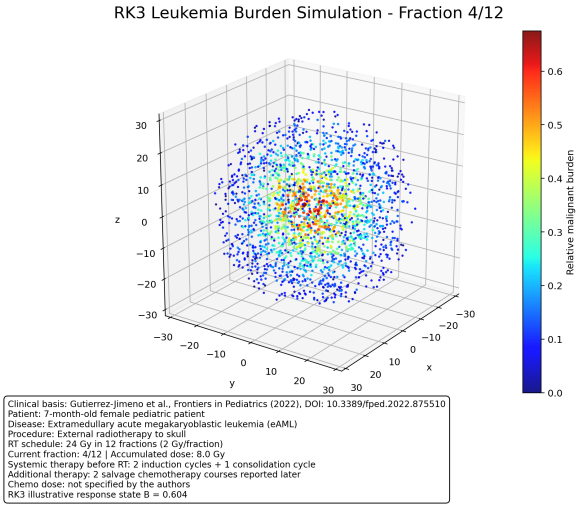


Figure 6. Fraction 4 of 12: contraction of the high-burden region after 8.0 Gy. Normalized global burden $B = 0.602$.

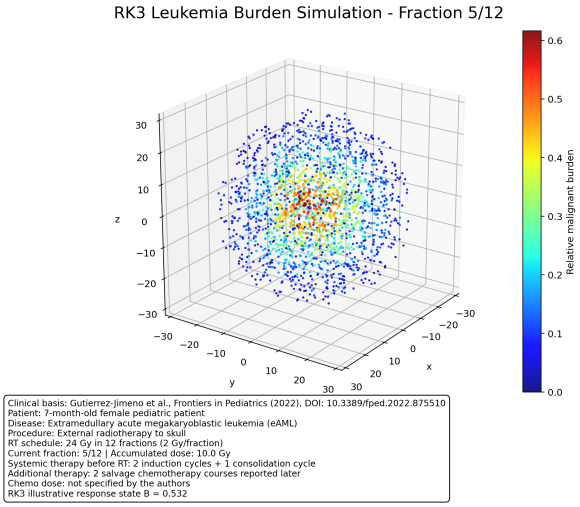


Figure 7. Fraction 5 of 12: intermediate response after 10.0 Gy. Normalized global burden $B = 0.531$.

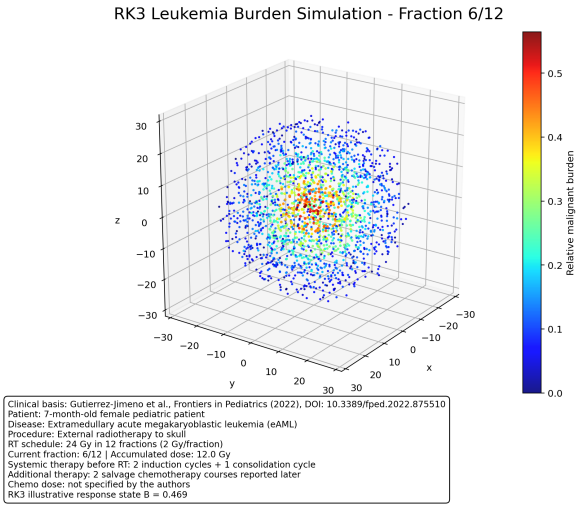


Figure 8. Fraction 6 of 12: mid-course response after 12.0 Gy. Normalized global burden $B = 0.468$.

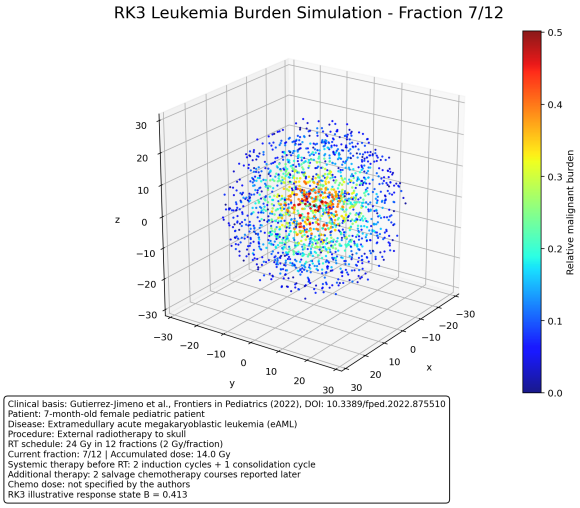


Figure 9. Fraction 7 of 12: late-intermediate response after 14.0 Gy. Normalized global burden $B = 0.412$.

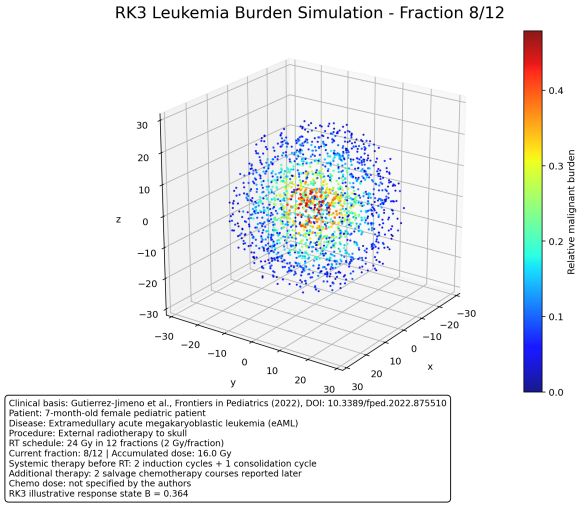


Figure 10. Fraction 8 of 12: reduced burden after 16.0 Gy. Normalized global burden $B = 0.363$.

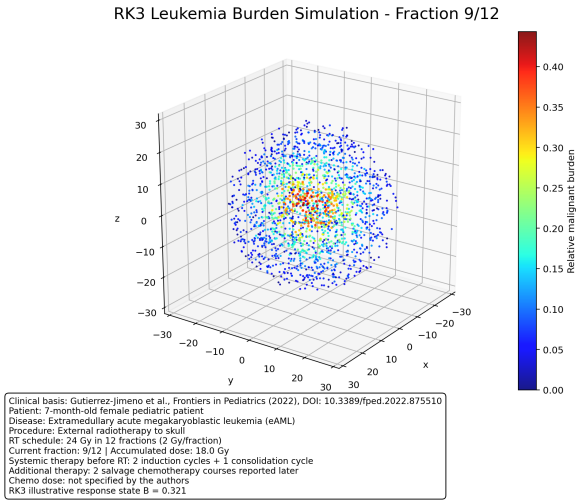


Figure 11. Fraction 9 of 12: advanced response after 18.0 Gy. Normalized global burden $B = 0.320$.

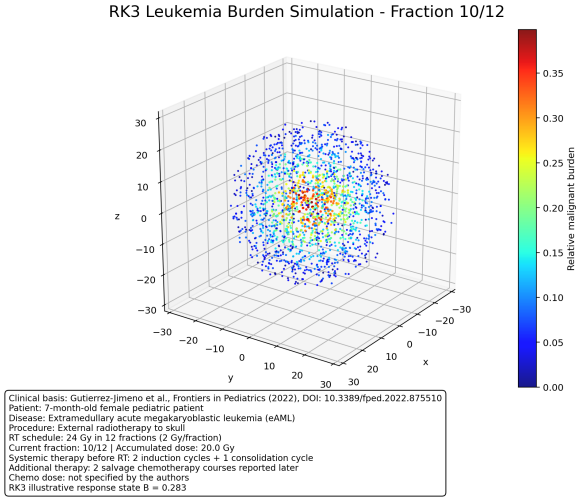


Figure 12. Fraction 10 of 12: marked reduction after 20.0 Gy. Normalized global burden $B = 0.282$.

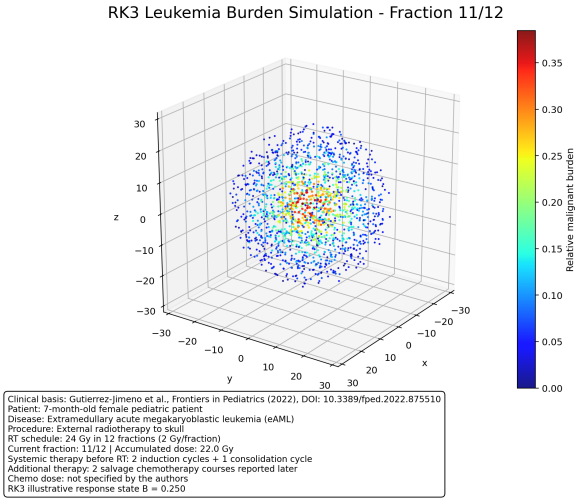


Figure 13. Fraction 11 of 12: near-final response after 22.0 Gy. Normalized global burden $B = 0.248$.

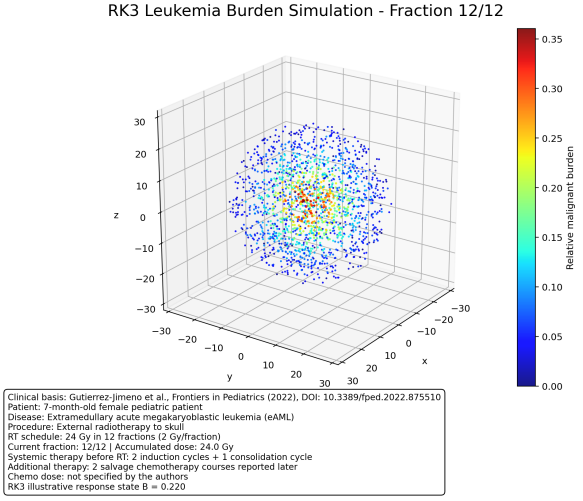


Figure 14. Fraction 12 of 12: final simulated burden after 24.0 Gy. Normalized global burden $B = 0.219$.

After the second fraction this warm-colored region is slightly smaller and the surrounding blue points become relatively more prominent.

In Figures 5 and 6 the high-intensity region shrinks further. The red core becomes more localized, and green and blue points occupy a larger part of the domain. The corresponding values of B follow the smooth exponential decay predicted by Eq. (59), as expected for a step size inside the stability interval.

Figures 7 and 8 correspond to the middle of the course, when about half of the initial burden remains. The distribution is visibly less intense and the region of maximum burden is smaller than in the first fractions.

In Figures 9 and 10 the warm-colored cluster becomes more compact, and the periphery of the cloud is dominated by low-intensity colors.

In Figures 11 and 12 the high-burden core is much smaller than in the first images, and the cloud as a whole is sparser and less intense.

Figures 13 and 14 show the end of the schedule. The cloud is clearly less intense than at the start and the red-orange region is much reduced; about 22% of the initial normalized burden remains after 24 Gy.

These images are not intended to reproduce the patient's anatomy or the full biology of the disease. They give a controlled, easily interpreted picture of burden reduction over the same number of fractions as in the clinical case, and thus translate a real treatment schedule into a reproducible computational experiment in which the numerical method has been derived and verified beforehand.

7 Conclusion

This study presented a complete derivation of the classical third-order Runge-Kutta method, from the initial-value problem through the Taylor expansion and the order conditions to the final formula, together with its absolute-stability interval on the negative real axis.

The reduced decay model allowed a direct numerical check. With the exact solution as reference, RK3 showed third-order convergence and the explicit Euler method first-order convergence. For the prescribed decay rate, the one-fraction step used in the clinical schedule satisfies the RK3 stability condition by a wide margin.

The biomedical application was defined as a normalized, subtype-independent burden model. The case of pediatric extramedullary acute megakaryoblastic leukemia supplied the radiotherapy schedule (24 Gy in 12 fractions), while the model parameter and the three-dimensional geometry are illustrative assumptions rather than patient measurements. Within these limits, the modeled burden decreased from 0.881 after the first fraction to 0.219 after the twelfth.

Future work should replace the reduced decay law with subtype-specific biological models, estimate proliferation, death and radiosensitivity parameters from longitudinal clinical data, include patient imaging, and test the scheme on coupled or stiff systems.

Data Availability Statement

The numerical results and figures were generated from the model and parameters described in this article. The clinical treatment schedule was taken from the published case report by Gutiérrez-Jimeno et al. [8]. No patient-level data or unpublished clinical records were accessed. The numerical scripts are available from the corresponding author upon reasonable request.

Funding

This work was supported without any funding.

Conflicts of Interest

The author declares no conflicts of interest.

AI Use Statement

The author declares that no generative AI was used in the preparation of this manuscript.

Ethical Approval and Consent to Participate

The present study involved only secondary analysis of information from a published case report and mathematical simulations; no new human or animal experiments were performed. Ethical approval and consent to participate were therefore not required.

References

[1] Daltveit, D. S., Morgan, E., Colombet, M., Steliarova-Foucher, E., Bendahhou, K., Marcos-Gragera, R., ... & Soerjomataram, I. (2025). Global patterns of leukemia by subtype, age, and sex in 185 countries in 2022. *Leukemia, 39*(2), 412-419. [CrossRef]

[2] Clapp, G., & Levy, D. (2015). A review of mathematical models for leukemia and lymphoma. *Drug Discovery Today: Disease Models, 16*, 1-6. [CrossRef]

[3] Chulián, S., Martínez-Rubio, Á., Rosa, M., & Pérez-García, V. M. (2022). Mathematical models of leukaemia and its treatment: a review. *SeMA Journal, 79*(3), 441-486. [CrossRef]

[4] Hassan, I. U., Javeed, S., Khan, M. S., Baleanu, D., & Bayram, M. (2026). Modeling, analysis and numerical simulation of chronic myeloid leukemia. *Theory in Biosciences, 145*(1), 7. [CrossRef]

[5] Parajdi, L. G., Bai, X., Kegyes, D., & Tomuleasa, C. (2025). A mathematical model of clonal hematopoiesis explaining phase transitions in chronic myeloid leukemia. *Mathematical Medicine and Biology: A Journal of the IMA, 42*(3), 253-288. [CrossRef]

[6] Bray, F., Laversanne, M., Sung, H., Ferlay, J., Siegel, R. L., Soerjomataram, I., & Jemal, A. (2024). Global cancer statistics 2022: GLOBOCAN estimates of incidence and mortality worldwide for 36 cancers in 185 countries. *CA: A Cancer Journal for Clinicians*, *74*(3), 229-263. [CrossRef]

[7] Kiwumulo, H. F., Muwonge, H., Ibingira, C., Kirabira, J. B., & Ssekitoleko, R. T. (2021). A systematic review of modeling and simulation approaches in designing targeted treatment technologies for leukemia cancer in low and middle income countries. *Mathematical Biosciences and Engineering*, *18*(6), 8149-8173. [CrossRef]

[8] Gutiérrez-Jimeno, M., Panizo-Morgado, E., Calvo-Imirizaldu, M., Galán-Gómez, V., Escudero-López, A., & Patiño-García, A. (2022). Case report: the value of genomic analysis in a case of megakaryoblastic leukemia with atypical initial manifestation. *Frontiers in Pediatrics*, *10*, 875510. [CrossRef]

[9] Hairer, E., Nørsett, S. P., & Wanner, G. (1993). *Solving Ordinary Differential Equations I: Nonstiff Problems* (2nd rev. ed., Springer Series in Computational Mathematics, Vol. 8). Berlin: Springer. [CrossRef]

[10] Roache, P. J. (2002). Code verification by the method of manufactured solutions. *Journal of Fluids Engineering*, *124*(1), 4-10. [CrossRef]

[11] Runge, C. (1895). Über die numerische Auflösung von Differentialgleichungen. *Mathematische Annalen*, *46*(2), 167-178. [CrossRef]

[12] Kutta, W. (1901). *Beitrag zur näherungsweisen Integration totaler Differentialgleichungen*. Teubner.

[13] Butcher, J. C. (1996). A history of Runge-Kutta methods. *Applied Numerical Mathematics*, *20*(3), 247-260. [CrossRef]



Matheus dos Santos Farias received the B.S. degree and a teaching qualification in physics from the Institute of Physics, University of São Paulo (IF-USP), Brazil, and a specialization in medical physics from Albert Einstein Israelite Hospital (HIAE), Brazil. He is currently pursuing the M.S. degree in nuclear physics at the Instituto de Pesquisas Energéticas e Nucleares (IPEN), São Paulo, Brazil. His research interests include delay differential equations, dynamical systems, mathematical modeling and numerical simulation in medical physics, proton therapy, and gold nanoparticles for nanobrachytherapy. He has clinical experience in diagnostic radiology, nuclear medicine, radiotherapy and radiation protection. He is a member of the APS, AAPM, ANS and the SIAM Activity Group on Dynamical Systems. (Email: matheusfariasfm@gmail.com)